SSC20-IX-01

Nytrox as a Volumetrically-Efficient, Green Oxidizer for SmallSat Hybrid Propulsion Systems

Stephen Anthony Whitmore
Utah State University
4130 Old Main Hill, UMC 4130, Logan UT 84322; (805) 435-797-2951
Stephen.Whitmore@usu.edu

Rob Louis Stoddard
Jacobs Engineering
Johnson Spaceflight Center, Houston TX 77058; 801-441-9496
stodz@gmail.com

ABSTRACT

Utah State University has recently developed a promising High-Performance "Green" Hybrid Propulsion (HPGHP) technology that derives from the novel electrical breakdown property of certain 3-D printed thermo-plastic materials. This property has been developed into a proprietary, power-efficient system that can be cold-started and restarted with a high degree of reli**ia**bility. HPGHP in the most mature form uses gaseous oxygen (GOX) as the oxidizer with 3-D printed acrylonitrile-butadiene-styrene (ABS) as the fuel. However, unless stored at very high pressures, GOX is a volumetrically inefficient propellant. A higher density "green" oxidizer alternative is highly desirable. Results of a preliminary test-and-evaluation campaign using "Nytrox," as volumetrically-efficient replacement for GOX are presented. Nytrox, a saturated solution similar to "laughing-gas" used for anesthesia, is blended by percolating *GOX* under pressure into medical grade nitrous oxide (N_2O) until the solution saturates. GOX in solution dilutes the ullage N_2O vapor content, increasing the thermal decomposition energy barrier by multiple orders of magnitude. Thus, risks associated with inadvertent thermal or catalytic N_2O decomposition are virtually eliminated. A 10-N hybrid thruster was first tested using GOX/ABS*ABS* as baseline propellants. Tests were repeated using Nytrox as a "drop-in" replacement for *GOX*. The system worked successfully with only minor modifications required.

INTRODUCTION

Over the past decade the USU Propulsion Research Laboratory has developed and refined a novel High-Performance "Green" Hybrid Propulsion (*HPGHP*) system as an environmentally sustainable replacement for hydrazine, a common but highly toxic and hazardous spacecraft propellant. This paper summarizes the results from the preliminary test-and-evaluation campaign where a 10-N HPGHP thruster, scaled for Smallsat applications was first tested using gaseous oxygen (GOX) and acrylonitrile butadiene styrene (*ABS)* as the baseline propellants. Tests were subsequently repeated using Nytrox, a blend of medical grade nitrous oxide (N_2O) and GOX as a high-density "drop-in" oxidizer replacement. Results from these tests demonstrate Nytrox as an effective replacement, exhibiting a slightly reduced specific impulse, but with significantly higher volumetric efficiency.

BACKGROUND

A recent study[1,2] by the European Space Agency Space Research and Technology Center (ESTEC) has identified two essential design elements to achieving low cost space access and operations; 1) Reduced production, operational, and transport costs due to lower propellant toxicity and explosion hazards, and 2) Reduced costs due to an overall reduction in subsystems complexity and overall systems interface complexity. The ESA/ESTEC study showed the potential for considerable operational cost savings by simplifying propellant ground handling procedures. Developing a non-toxic, stable “green” alternative for most commonly used toxic or potentially-hazardous propellants was highly recommended by the ESTEC study.

Hybrid Rockets as a "Green" Propulsion Alternative

The inherent safety and environmental friendliness of hybrid rocket systems have been known for several decades.[3] Hybrids have the potential to act as an ideal "green" alternative for many of the current generation of toxic or hazardous propellants. Because hybrid systems only require a single fluid flow path, they are of similar complexity to monopropellant systems; but with significantly higher performance. In fact, when properly optimized, hybrid systems have the potential to provide

the same performance as significantly more complex bi-propellant liquid systems. While hybrid rocket systems have been considered for applications ranging from large launch systems to nanosatellites, they have not found a real niche with the space-launch and space propulsion industries. Solid and liquid bi-propellant systems have been under development for more than seven decades and the state of technology development for hybrid systems is rather immature by comparison.

As the Technology Readiness Level(TRL) matures, small hybrid systems offer the potential to fill an unmet and growing need for advanced propulsion both in-space and as launch stages for the emerging SmallSAT market. Hybrid rockets offer particular utility for the upper stages of a nano-launch vehicle. Although a hybrid rocket will increase the overall system dry mass compared to a solid-propellant motor, the capabilities to throttle, shut-down on demand, coast, and relight the motor, will offset any loss in performance of the stage. Such a "smart-stage" would not only provide ΔV to enable the payload to reach orbit; but can also serve as an on orbit maneuvering system that allows precise placement of the payload. Such a system could also provide extensive capabilities for endo-atmospheric maneuvering for a variety of defense applications.

Hybrid Rocket Low-Power Arc-Ignition System

Historically, due to the lack of a reliable non-pyrotechnic, multiple-use ignition method, hybrid rockets have never been seriously considered as feasible for in-space propulsion. Hybrid rockets are “safe” due to the relative propellant stability; however, this stability makes hybrid rocket systems notoriously difficult to ignite. The hybrid rocket ignition source must provide sufficient heat to pyrolize the solid fuel grain at the head end of the motor, while simultaneously providing sufficient residual energy to overcome the activation energy of the propellants. Conventional solid-propellant ignition systems use pyrotechnic or “squib” charges to ignite a secondary solid-propellant motor whose high-enthalpy output rate initiates the full motor combustion.

Such high-energy devices often come with a suite of environmental and objective risks, and operational challenges. Pyrotechnic charges are extremely susceptible to the Hazards of Electromagnetic Radiation to Ordnance (HERO),[4] and large pyrotechnic charges present a significant explosion hazard that is incompatible with many launch opportunities. Most importantly, for nearly all applications pyrotechnic ignitors are designed as "one-shot" devices that do not allow a multiple restart capability. Thus the great potential for restartable upper stages or in-space maneuvering systems using hybrid propulsion remains largely unrealized. An operational hybrid system with multiple restart capability does not currently exist.

Whitmore et al (2015)[5] and Whitmore (2017)[6] discovered a solution to the aforementioned restartability issue by leveraging the unique electrical breakdown properties of certain thermoplastics like acrylonitrile butadiene styrene (ABS), when processed using a type of additive manufacturing known as Fused Deposition Modeling (FDM).[7] Under normal conditions, ABS possesses a very high electrical resistivity and is not generally considered as an electrical conductor. However, as FDM-processed ABS is subjected to a moderate electrostatic potential between electrodes embedded in the material, the layered FDM structure concentrates electrical charges at points along the surface. These charge concentrations carve a conduction path along the material surface. Joule heating from current flowing along this char-path provide sufficient heat to pyrolyze a small amount of fuel material.[8]

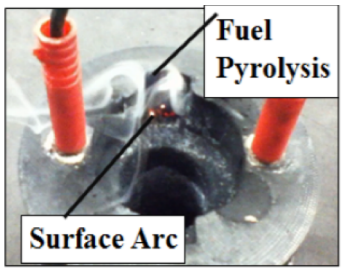

Figure 1. Inductive Pyrolysis of 3-D Printed ABS Fuel.

Because Joule heating pyrolizes a small mass of fuel material, when an oxidizing flow is introduced at oxygen partial pressures above two atmospheres. (Ref.[13]) Figure 1 shows a typical pyrolysis event, where the ablated hydrocarbon vapor results from the inductive arc carving a path across the fuel surface. The pyrolyzed material seeds combustion when an oxidizing flow is introduced. Typical startup sequences require less than 2 joules; and once started, the system can be sequentially fired with no additional energy inputs required.[9] The number of possible ignitions limited only by the amount of fuel.

The patented system[10] has been engineering to a high level of reliability with multiple prototypes of thrust levels varying from 4.5 to 900 N having been tested. (Ref. [11]) A flight-weight 25-N thruster system has been extensively vacuum tested.[11] On 25 March, 2018 a flight experiment containing a 10-N prototype of this thruster system was launched aboard a two-stage Terrier-Improved Malemute sounding rocket from Wallops Flight Facility. The launch achieved apogee of 172 km, allowing more than 6 min in a hard-vacuum environment above the Von-Karman line. The thruster was successfully fired five times Whitmore and Bulcher (2018)[12] report the details of this flight test experiment.

Additive manufacturing changes the electrical breakdown properties, and when printed materials are presented with a sufficiently high, low-current voltage, electrical-arcing along the layered surface pyrolizes material and seeds combustion when an oxidizing flow is introduced.[13] Typical startup sequences require less than 2 joules; and once started, the system can be sequentially fired with no additional energy inputs required. (Ref. [9])

Current Status of the HPGHP Technology

In its most mature form *HPGHP* uses gaseous oxygen (GOX) as the oxidizer, and although, *GOX* is a mass efficient oxidizer; it is volumetrically inefficient due to its low specific gravity. In order to increase the system volumetric efficiency, a two-phase blend of nitrous oxide (N_2O) and *GOX,* "Nytrox," has been engineered as a higher-density "drop-in" replacement. Nytrox is similar to "laughing-gas" used for anesthesia applications, and is blended by percolating *GOX* under pressure into N_2O until the solution reaches saturation. The process is analogous to the creation of soda-water using dissolved carbon dioxide. The molecular oxygen in solution dilutes the N_2O ullage vapor and increases the required decomposition energy barrier by multiple orders of magnitude. Thus, risks associated with inadvertent thermal or catalytic N_2O decomposition are virtually eliminated.

Nitrous Oxide as a Volumetrically-Efficient Hybrid Oxidizer

As described earlier, the low-power arc-ignition system is a key enabling technology for in-space hybrid propulsion. To date, however, the vast majority of development of this system has relied on the use of gaseous oxygen as the oxidizer. Gaseous oxygen is an excellent oxidizer and the proposal team has significant experience with testing of small hybrid thruster systems using GOX. GOX is entirely "green" and can be quite safely worked with at pressures below 2500 psig, as long as appropriate systems cleanliness standards are adhered-to.[14] Unfortunately, GOX even when stored at high pressure has too low of a density to be volumetrically efficient for space missions requiring even moderate ΔV levels.

Nitrous Oxide is inexpensive, readily available, and long been considered the "standard" oxidizer for hobby-rocket hybrid enthusiasts. Nitrous Oxide exists as a two-phase saturated liquid below its critical temperature of 36.4 °C. At room temperature ($20\ ^oC$) N_2O has a vapor pressure of approximately *5,050 kPa (732 psia),* and a liquid-phase density *of 0.785 g/cm*^{3}. This density is equivalent to gaseous oxygen stored at approximately 59,800 kPa (8,670 psia), or a factor of nearly 12 times larger than the corresponding N_2O vapor pressure. Such a high *GOX*-storage pressure value will require a far heavier tank weight compared to an equivalent N_2O tank. Thus, for flight systems requiring even moderate amounts of ΔV, the differences in the tank weights alone will more than make up the mass losses due to the lower specific impulse (I_{sp}) contribution of N_2O compared *GOX*.

As a saturated liquid N_2O is relatively benign, and in *pure form* N_2O is classified as non-toxic, non-explosive, and non-flammable as by the US. Occupational Safety and Health Administration (OHSA).[15]

Nitrous oxide does have an exothermic strong decomposition reaction of the form

$$N_2O = N_2 + \frac{1}{2}O_2 \quad \uparrow \quad heat \qquad (1)$$

Releasing up to *1864 kJ* of energy for each kilogram of fluid that is decomposed. In pure form liquid phase N_2O is nearly impossible to detonate.[16] Even as a two-phase fluid with both liquid and vapor phases present, N_2O has a large activation energy, E_a, for thermal decomposition, 5682 kJ/kg, and N_2O vapor must be heated to temperatures near 1000 °C in order to induce thermal decomposition.[17]

However, when N_2O vapor is contaminated by a small amount of "seed" hydrocarbon material, the relative stability is lowered and E_a drops significantly, and thermal decomposition can occur at temperatures below 350 °C. In effect, the addition of hydrocarbon material to nitrous oxide catalyzes the decomposition event.[18] Figure 2 illustrates the concept where "hydrocarbon-seeding" lowers the activation energy.

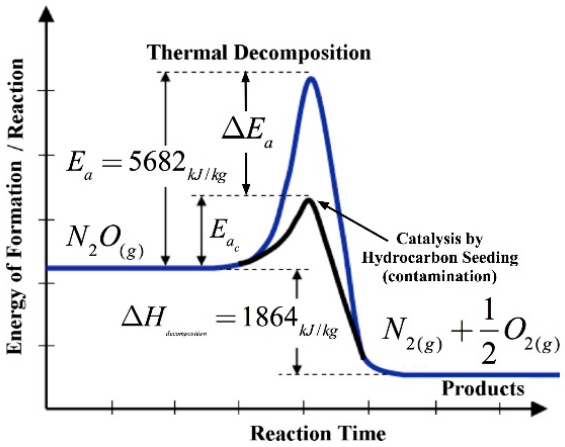

Figure 2. Hydrocarbon seeding reduces the N_2O decomposition energy barrier.

Also, because N_2O is a highly polar molecule and an exceptionally good solvent, it readily picks up and dissolves hydrocarbons or other contaminating materials that may be exposed to the flow path. Since only a small amount of contamination is needed to catalyze decomposition, this physical property further exacerbates the potential safety hazards associated with N_2O propulsion applications.

For flight applications, close-coupling of the oxidizer tank with the motor case creates a significant chance of introducing contamination into the thrust chamber. As the motor burns and nitrous oxide is depleted, adiabatic cooling forces a significant drop in the tank vapor pressure. This internal pressure drop provides the opportunity for backflow across the injector, allowing hot hydrocarbon gasses to enter the oxidizer feed lines and possibly the lower portion of the tank itself. The result is a significant potential for a run-away decomposition reaction. A notable number of accidents resulting from runaway N_2O decomposition events have occurred. Karabeyoglu et al. (2008) [18] presented a summary of nine verified accidents related to inadvertent, uncontrolled nitrous oxide decomposition events.

Mitigating the Nitrous Oxide Decomposition Hazard

Fortunately, it appears following procedures developed by the medical and dental anesthesia community offers a strong mitigation to this decomposition hazard.[19] In a manner directly analogous to creation of soda-water using dissolved carbon dioxide, an N_2O/O_2 hybrid solution, referred to as Nytrox for the remainder of this paper, is created by bubbling gaseous O_2 under pressure into liquid N_2O until the solution reaches saturation. The oxygen in solution displaces much of the nitrous oxide vapor in the tank ullage, significantly reducing the potential for a decomposition reaction, and allows "laughing gas" to be safely worked with in a clinical environment.

Because O_2 in solution dilutes the N_2O vapor in the tank ullage, the required ignition energy E_i, defined as the minimum energy required to initiate a deflagration wave, is significantly increased. Assuming a spherical flame kernel, when the input energy is smaller than E_i, the resulting flame front decays rapidly because the released heat diffuses away from the surface faster that can be replaced by the decomposing material in the kernel volume. Dilution of the N_2O vapor with O_2 effectively increases the kernel volume, reducing the energy density. The diluent gas also acts to absorb heat, further quenching the reaction.

The data of Figure 3 illustrate the effect of the O_2 dilution in the Nytrox vapor phase upon E_i. These data are extrapolated from Karabeyoglu (2014)[20] and Borisov and Troshin.[21] For this calculation, Reference [20] assumes a spherical ignition kernel. Fig. (3a) plots the minimum ignition energy as a function of ullage O_2 mass fraction for pressure levels varying from 40 to 100 atmospheres. Fig. (3b) plots the ratio of the ignition energy at a given O_2 mass concentration to the value for pure N_2O vapor at the same pressure level. This ratio is referred to as the ignition energy amplification factor, E_{if}.

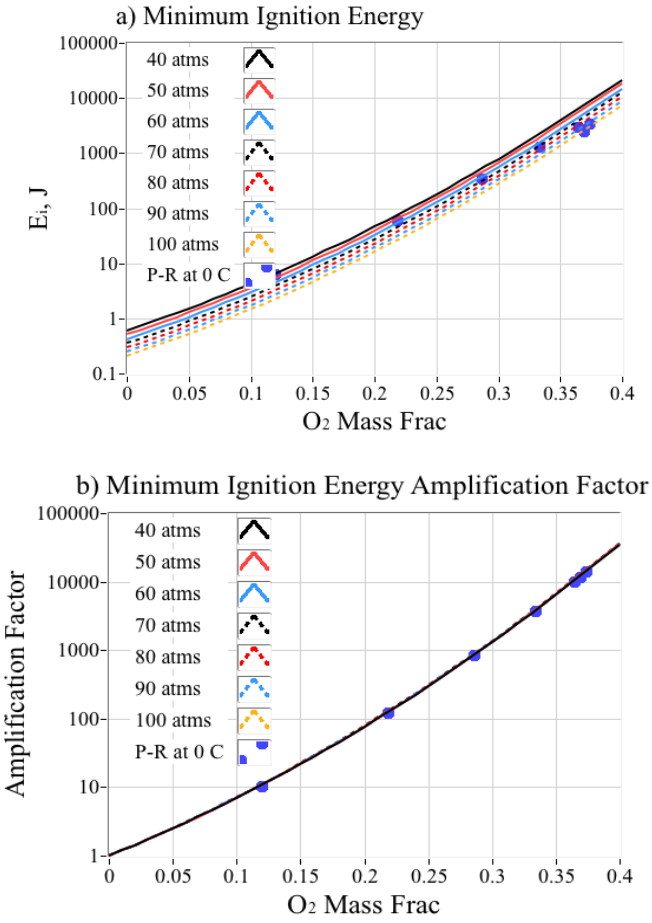

Figure 3. Minimum Ignition Energy E_i per Pram of Fluid for Nytrox Mixtures at 7 Storage Pressure Levels.

Note that even small amount of O_2 in the vapor phase significantly increases the required decomposition energy. For example, with an O_2 dilution of only 20%, the require decomposition energy rises from less 1 Joule to greater than 25 Joules, an amplification factor E_{if} of two orders of magnitude. At 40% dilution the E_i grows to nearly 10 kJ, or an amplification factor of more than 10,000. This buffering effect significantly increases the handling safety for Nytrox, and it may be reasonably concluded that ignition cannot be achieved by any conceivable inadvertent ignition source.

Effects of Temperature and Pressure Upon the Equilibrium O_2 Concentration and Mixture Density

Figure 4 plots the vapor/liquid isotherm diagrams for a saturated "Nytrox" solution. Figs. (4a) and (4b) plot the O_2 mass concentrations for the vapor and liquid phases, respectively. Figs. (4c) and (4b) plot the corresponding vapor and liquid phase densities. The various curves represent the isotherm levels varying from −30 °C to 30 °C. The 0 °C isotherm is highlighted as the solid blue line for both the liquid and vapor segments of the chart.

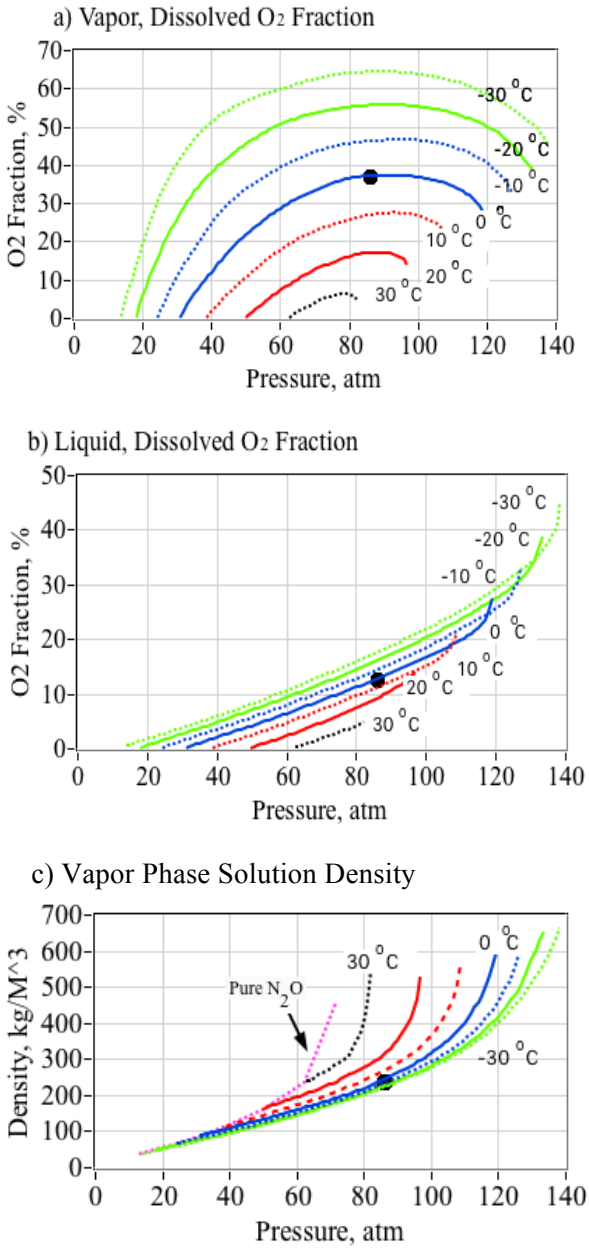

Figure 4. Nytrox Vapor/Liquid Isotherm Plots, for O_2 Mass Fraction and the Resulting Phase Densities.

Reading the diagrams of Fig. (4), at 0 °C and approximately 86 atmospheres (8745 kPa), there exists a "sweet spot" where the concentration of oxygen in the vapor-phase is a maximum (note that the pressure required to hold the O_2 in solution is significantly higher than the natural vapor pressure of N_2O, approximately 30 atmospheres at 0 °C).[22] This optimal point, noted by the circular symbol on the graphs, shows that the vapor phase contains approximately *37% O_2* mass fraction, while the O_2 mass fraction in the liquid phase lies at just below 13%. This near-optimal point allows for the maximum proportion of vapor dilution while maintaining the highest possible density for the liquid phase.

Near the "sweet spot" where the vapor O_2 mass concentration peaks at 0 °C and 86 atmospheres, the liquid-phase density is approximately 780 kg/m^3. At this point the liquid-phase Nytrox density is slightly lower than for saturated nitrous saturated oxide at the same temperature, or approximately 900 kg/m^3. Thus, at the optimal point Nytrox is only 13% less dense than pure nitrous oxide. At a higher storage pressure of 120 atmospheres (12,160 kPa) and 0 °C, the percentage of N_2O in the liquid-phase drops to around 70% with a corresponding density of only 600 kg/m^3. This difference amounts to a density drop of more than 40% compared to saturated N_2O at the same temperature. This behavior occurs because the nitrous oxide and oxygen become mutually dissolved in each other, and as the oxygen content in solution rises, the density drops. Thus, maintaining the storage pressure near the best value of 80 atmospheres is essential to achieving volumetric efficiency with Nytrox.

The calculations of Fig. (4) were performed using the Peng–Robinson[23] two-phase state-equation for binary

solutions. The mixing rule used to combine the O_2 and N_2O binary components is based on the model of Zudkevitch and Joffe.[24] At phase equilibrium, the fugacity (for the purposes of this model the fugacity may be defined as the pressure of an ideal gas which has the same Gibbs free energy as the real gas at the same temperature. Fugacity—the "tendency to escape" from solution—is the measure of a mixture component's values for the liquid and vapor phases of each fluid component are equal. The implemented numerical algorithm that performs these calculations follows the procedure laid out by Karabeyoglu. (Ref. [20])

Comparing the Theoretical Performance of the Nytrox/ABS to GOX/ABS Hybrid

Figure 5 compares the performance of the hybrid propellants using 5 different Nytrox blend options. The calculations of Fig. (5) were performed using the industry-standard NASA Chemical Equilibrium Program (CEA).[25] Here ABS is the fuel component with a notional composition of 33%, 33%, and 34% acrylonitrile, butadiene, and styrene monomer mole-fractions. The propellants are assumed to be initially stored at *0 °C* before entering the combustion chamber.

The plotted curves with differing colors compare pure *GOX* (*black*) and *N_2O (red)*, against Nytrox with 3 different liquid-phase *O_2* mass proportions, *90% N_2O/ 10% O_2 (blue), 70% N_2O/ 30% O_2 (green), and 50% N_2O/ 50% O_2 (violet)*. For notational simplicity the Nytrox blends are referred by the mass-percentage of *N_2O* in the liquid-phase of the solution; *GOX, N_2O, Nytrox90, Nytrox70, and Nytrox50,* etc. For each Nytrox color grouping the different line styles represent 6 different combustion pressure levels varying from *690 to 3450 kPa* (100 to 500 psia.).

Parameters plotted on Fig. (5) include *(a)* characteristic velocity *c^**, *(b)* vacuum *I_{sp}*, *(c)* specific gravity, and *(d)* impulse density *ρI_{sp}*. For this analysis impulse density is defined as the product of the mean propellant density and the vacuum specific impulse, expressed in unit of *N-s/liter*. The vacuum *I_{sp}* calculations allow a 25:1 nozzle expansion-ratio, with the combustion products frozen at the nozzle throat. For comparison purposes *I_{sp}* and *ρI_{sp}* of monopropellant-hydrazine are also plotted on Figs. (6b) and (6d).

The low *GOX* storage density at *86 atms* results in the lowest impulse density for all of the hybrid oxidizers. Using pure *N_2O* gives the best volumetric efficiency, but results in the lowest specific impulse and requires significantly more oxidizer at the optimal *O/F ratio*. The curve corresponding to the *Nytrox 90* mixture gives the best compromise with a distinct *ρI_{sp}* optimum occurring at an *O/F* ratio of approximately 4. Also note the vacuum *I_{sp}* for each hybrid oxidizer significantly exceeds that of hydrazine.

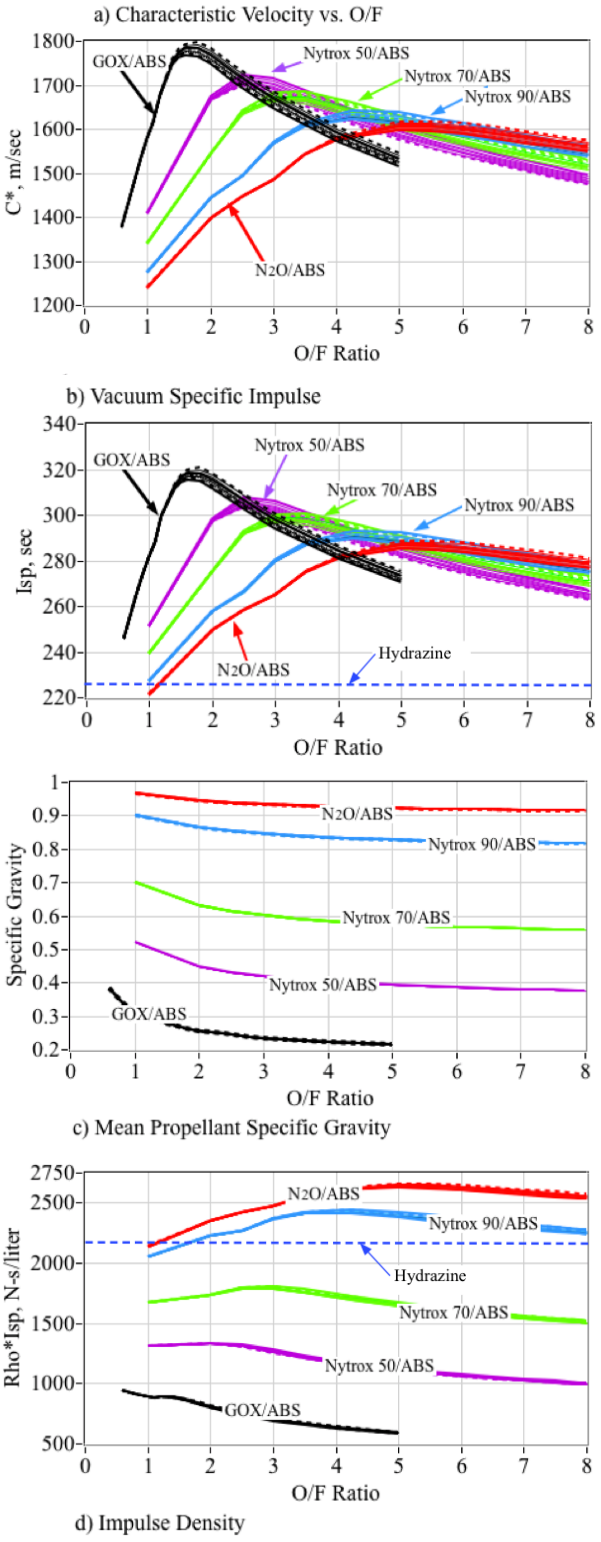

Figure 5. Performance of 3 *Nytrox* Concentrations Compared Against Pure *N_2O* and *GOX* as Oxidizer.

The mean specific gravity of the combined propellants is calculated by

$$\overline{s}_g = \frac{1}{\rho_{H_2O}} \cdot \left(\frac{\rho_{Oxidizer} \cdot \rho_{HTPB} \cdot (O/F+1)}{\rho_{HTPB} \cdot O/F + \rho_{Oxidizer}} \right). \quad (2)$$

In Eq. (2) ρ_{H2O} is the density water at 20 ^{o}C, $\rho_{oxidizer}$ is the oxidizer density, ρ_{fuel} is the fuel density, and *O/F* is the oxidizer-to-fuel ratio of the propellants. The specific gravity calculation for *GOX* assumes a storage pressure of *86 atm (8745 kPa) at 0 ^{o}C*. The specific gravity calculation for pure N_2O uses the saturation liquid density *at 0 ^{o}C* from Ref. [22]. The specific gravity calculation for the Nytrox blends are taken from the Peng-Robinson model of Fig. (4), using liquid-density values for the appropriate N_2O/O_2 mass proportions. The associated density of the assumed ABS fuel blend is *1.04 g/cm^3*.

Finally note that chamber pressure has only a second order effect upon the comparative peformances of the propellants, with the highest chamber pressure (*3450 kPa*) exhibiting appriximately 5% greater c^* and I_{sp} than the lowest chamber pressure (*690 kPa*). Chamber pressure has essentially no effect upon impulse density. Thus, even though the results to be presented later in this paper consider a small thruster system operating at relatively low chamber pressures, the results have a wider range of applicability, showing that an increased chamber pressure does little to aid the system performance.

Summary of Nytrox Properties and Safety Advantages Compared to Pure Nitrous Oxide

As summarized by Ref. [20], the key advantages associated with using Nytrox mixtures to replace N_2O as a hybrid oxidizer are:

(1) Nytrox is much safer than pure N_2O because vapor phase has significant O_2 concentration, thereby increasing the minimum ignition energy E_i by three or four orders of magnitude,

(2) The multiple order of magnitude increase in E_i using Nytrox allows for safe self-pressurization with high fluid densities.

(3) Self-pressurization greatly simplifies the system design and eliminates the need for a heavy, separate pressurant system using helium or nitrogen.

(4) Due to the oxygen in solution Nytrox allows improved I_{sp} performance compared to pure N_2O.

(5) From Figure 4, at the optimal pressure level of 86 atmospheres, the Nytrox liquid density at 0°C is higher than GOX by a factor approximately 6.4, and allows for a significant improvement in the overall volumetric efficiency of the propellants.

(6) Maintaining the storage pressure near 86 atmospheres at 0 °C is essential to achieving best volumetric efficiency with Nytrox.

(7) The optimal O/F ratio is significantly reduced when using Nytrox, allowing a larger proportion of the total impulse to be delivered by the high-density fuel component, in this case ABS.

EXPERIMENTAL APPARATUS AND TEST PROCEDURES

As described in the introduction section, a primary objective of this testing campaign was to demonstrate the effectiveness of Nytrox as a "drop-in" replacement for *GOX* in the *HPGHP* system. This section discusses the process for manufacture of the Nytrox solution, followed by a description of the test article, experimental apparatus, and hot-fire test procedures. The legacy hybrid thruster used for this evaluation was previously optimized for GOX as the oxidizer. The presented discussion is a top-level summary. Whitmore and Bulcher [9], Stoddard,[26] and Whitmore and Stoddard[27] present the analytical methods, test apparatus, instrumentation, test procedures, and analysis methods in significantly greater detail.

Nytrox Solution Processing

For this study highly-purified grades[28] of N_2O and *GOX* were used to ensure that the resulting Nytrox mixture was free from contaminants and any other possible catalytic agents. The objective of the developed procedure is to generate a Nytrox solution that lies near the previously-described "sweet spot," at *86 atms* pressure where the solution possesses a maximum concentration of oxygen in the vapor phase. The resulting "*Nytrox87*" solution has a vapor phase O_2 concentration of 37%, and a liquid phase O_2 concentration of approximately 13%. The liquid-phase *Nytrox 87* solution has a density of approximately 0.*780 g/cm^3*. Using the ideal gas law, GOX at the same temperature and pressure would have a density of 0.123 *g/cm^3,* or only 16% as dense

Figure 6 shows the percolation apparatus block diagram. For this test campaign the procedure consists of filling the 4.5 kg-capacity (10 lbs) Nytrox run tank half-full with nitrous oxide. During filling flow is passively initialed by placing the empty Nytrox run tank in an ice bath to lower the temperature to 0°*C*, while the N_2O service tank is kept at room temperature. The temperature difference lowers the vapor pressure of the

run tank fluid, creating a pressure difference that motivates in fluid flow.

Once the nytrox run tank is filled with the desired mass of nitrous oxide, the three-way valve is moved isolate the N_2O fill tank, and to allow oxygen to begin flowing into the nytrox run tank. The *GOX* regulator set pressure is maintained at 86 atmospheres throughout this process. A dip-tube in the run tank allows GOX to bubble up through the nitrous oxide. During passage through the liquid N_2O, oxygen dissolves into solution and also droplets of nitrous oxide are carried up into the gas phase.

Equilibrium conditions are noted when the storage tank settles at a constant weight and internal pressure. With the fill-regulator set at 8720 kPa (*86 atm absolute pressure*), the process takes about 2 hours to reach equilibrium. After the Nytrox is blended at the desired density, the serviced Nytrox run tank is stored at *–15 °C* temperatures in a portable freezer to keep vapor pressures low and ensure a minimal amount of N_2O vapor in the tank ullage.

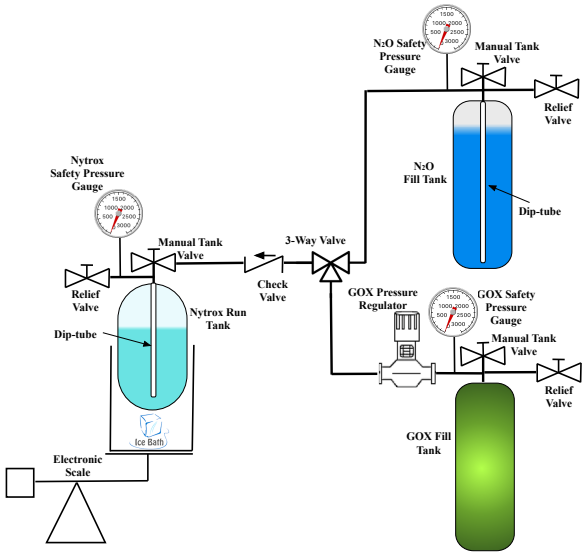

Figure 6. Nytrox Percolation Apparatus Block Diagram.

Thrust Chamber

As described previously, a legacy *GOX/ABS* prototype of Ref. [9] was reconfigured this testing campaign. Figure 7 presents the details of the thrust chamber assembly showing the top and side view schematics and the major system assembly components; *i*) graphite nozzle, ii) nozzle retention cap, iii) motor case, iv) 3D printed fuel grain with embedded electrodes, v) insulating phenolic liner, vi) chamber pressure fitting, and vii) single-port injector cap. The 38-mm diameter motor case, constructed from 6061-T6 aluminum, was procured commercially.[29]

a) Top and Side-View Schematics

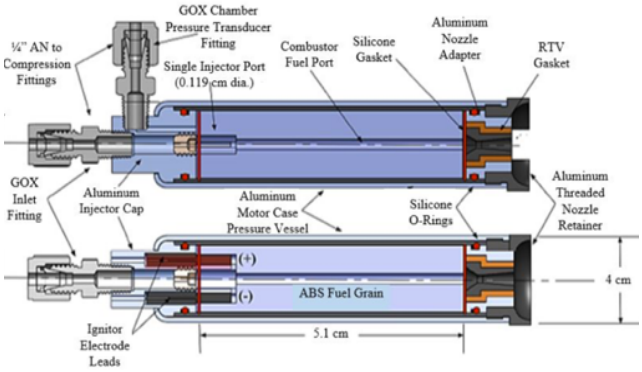

b) Components

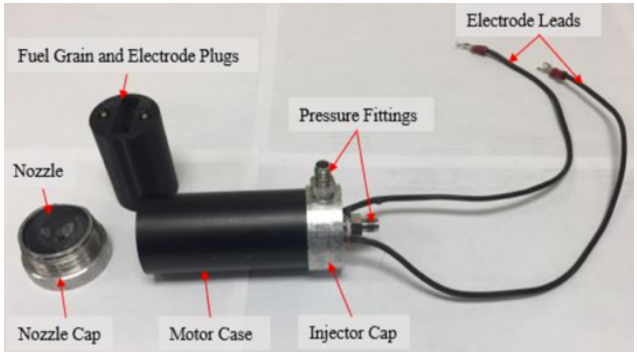

Figure 8. Thrust Chamber Assembly.

Table 1: Page Margins for Letter and A4 Submissions

Table 1 summarizes the thrust chamber component geometry specifications, including the injector, fuel grain, motor case, and nozzle.

Table 1: Motor Component Geometry Specifications.

Injector	Fuel Grain	Motor Case	Nozzle
Single Port, Brass	3-D FDM ABS	6061-T6 Al	Graphite
Dia 0.127 cm	External Dia. 3.168 cm	External Dia. 3.8 cm	Throat Dia. 0.345 cm
Length 1 cm	Port Dia. 0.53 cm	Wall Thickness 1.5 mm	Exit Diameter 0.483 cm
	Length 5.1 cm	Length 7.92 cm	Exp. Ratio 2.07
	Weight 45 g	Weight 34 g	Conical Exit angle 5^0

Arc Ignition System

Figure 9 shows the details of the arc-ignition system. Fig. (9a) shows the fuel grain head end layout with flow impingement shelves and embedded electrodes in the 3-D printed ABS fuel grain. Fig. (9b) shows the ignition system electronics schematic. The ignition system power processing unit is based on the UltraVolt® line of high-voltage power supplies (HVPS).[30] The HVPS provides a current-limited (30 mA) high voltage output of up to 1000 V or 30 Watts total output. Depending on the impedance on the arc path between the ignitor electrodes, the dissipated voltage typically varies between 100 and 400 volts. Ignition power to the thruster is initiated by sending a TTL-level activate logic bit to the HVPS.

a) Fuel Grain Head-End Layout

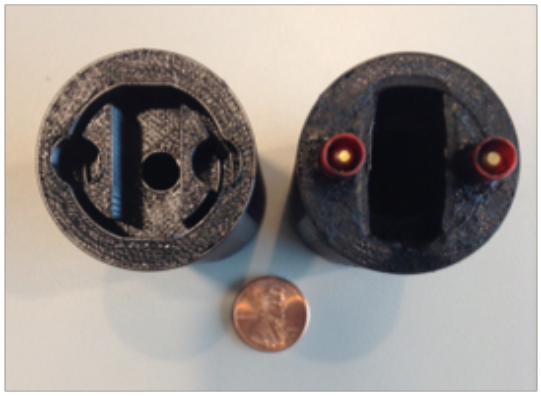

b) Ignition System Electronics Schematic

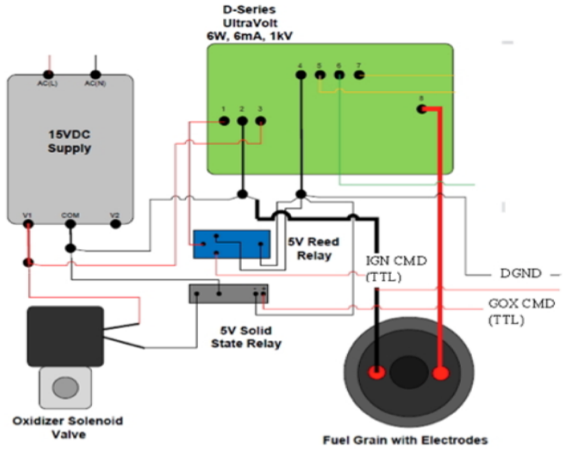

Figure 8: HPGHP Arc-Igniton System.

Test Stand Apparatus and Instrumentation

Figure 9 shows the test motor assembled and mounted to the test stand. For this configuration support members allow bending along the direction of thrust to prevent them from interfering with the measured load.

Figure 10 shows the piping and instrumentation diagram (P&ID) of the test systems. The test stand measurements include Venturi-based oxidizer massflow measurements, load-cell based thrust measurements, chamber pressure, and multiple temperature readings at various points along the flow path. The system was configured to allow rapid cycling between Nytrox and GOX using s 3-way valve. Directly aft of the thrust chamber lies the solenoid actuated oxidizer run-valve.

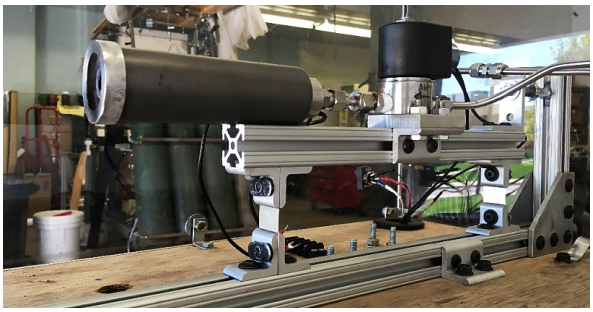

Figure 9. Thrust Chamber Mounted to Load-Balance Test Sled.

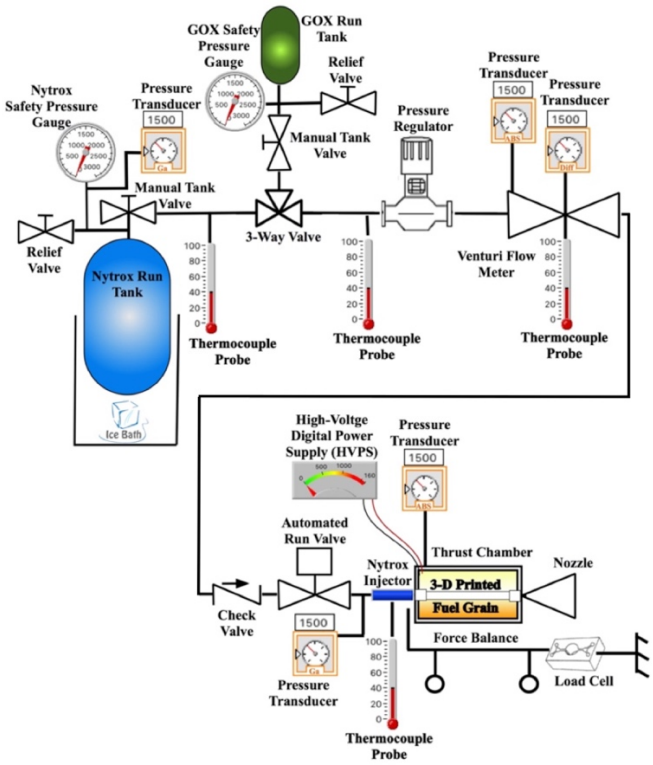

Figure 11. Hot-Fire Test Apparatus Piping and Instrumentation Diagram.

Test Procedures were nearly identical for both the GOX baseline and Nytrox tests. Pre-test measurements included fuel grain weight and port diameter, measured

at both the top and bottom of the fuel port. The nozzle throat and exit plane diameters were also measured. Finally, the initial oxidizer run-tank tank weight, pressure, and temperature were measured. All data were logged on a spreadsheet for post-test analysis.

The upstream oxidizer flow regulator feed pressure was manually set to approximately 22 atmospheres (2230 kPa) in order to choke the injector and ensure a constant oxidizer massflow throughout the burn. For the two-phase Nytrox flow this pressure level also proved to be sufficiently high to quasi-choke the injector, and significantly reduced the risk of incurring injector-feed coupling instabilities during combustion.

In order to ensure Nytrox ignition reliability, the HVPS was activated sending power to the fuel grain electrodes one second before the oxidizer run valve was opened. Once the run valve opened, then HVPS power to the electrodes was continued to overlap for another 1 second. Since the required power was so small, no attempt to shorten or optimize the "spark" length or overlap time was performed for this test series. For this test series, the motor run valve was programmed to open for a prescribed amount time that varied from 1 to 4 seconds. The motor would snuff immediately after closure of the run valve.

Allowing for a safety margin to prevent motor-case burn through, one fuel grain allows for 8 seconds of total burn time. Thus, on a single fuel grain a typical test series would prescribe four tests of 2 seconds each, or two tests of 4 seconds each. Following each burn, the weight and geometry measurements described in the previous paragraphs were repeated and logged for post-test analysis.

Initially, baseline tests were performed using gaseous oxygen as the oxidizer. Following the baseline tests, the *GOX* tank was swapped for the run tank filled with the processed Nytrox. A commercial Holley Nitrous Oxide Systems (*NOS*®)[31] storage tank was used as the nitrous oxide run tank. In order to simulate a true operational environment, during hot-fire testing the Nytrox tank, stored at *-15 °C* was gradually allowed to warm to ambient conditions. Other than the change in oxidizer and storage tank, the test assembly remained identical for both oxidizers.

DATA ANALYSIS METHODS

This section summarizes the analytical methods used to calculate key derived-parameters from the raw test data. Mass-flow based calculations include 1) oxidizer massflow, 2) oxidizer-to-fuel ratio, and 3) equivalence ratio. Key performance parameters calculated from the raw data include 1) combustion efficiency, 2) thrust coefficient, 3) specific impulse, 4) characteristic velocity, and 5) impulse density.

Although the inline Venturi measures the oxidizer massflow in real-time, the test stand was not configured to directly measure the fuel massflow. Instead, before and after each hot-firing the fuel grains were weighed to give the total fuel mass consumed during the test. As will be described later in this section, these mass measurements were used to anchor the "instantaneous" fuel massflow rates, calculated as the difference between the nozzle exit and oxidizer massflows,

$$\dot{m}_{fuel} = \dot{m}_{total} - \dot{m}_{ox} \quad . \tag{3}$$

Knowing the nozzle throat area A^* and the plume exhaust gas properties, the nozzle exit (total) massflow at each time point was calculated from the measured chamber pressure time history P_0, using the 1-dimensional choking massflow equation,[32]

$$\dot{m}_{total} = A^* \cdot P_0 \cdot \sqrt{\frac{\gamma}{R_g \cdot T_0} \cdot \left(\frac{2}{\gamma + 1} \right)^{\frac{\gamma+1}{\gamma-1}}} \quad . \tag{4}$$

The calculation of Eq. (4) assumes the flow composition is frozen at the nozzle entrance, (Anderson, [32], pp 659-661) and nozzle erosion during the burn.

A table of thermodynamic and transport equilibrium properties of the GOX/ABS and Nytrox/ABS exhaust plumes were calculated using the previously-described CEA code (Ref. [25]) with chamber pressure P_0 and mean *O/F* ratio as independent look up variables. For each data point in the burn time history, the two-dimensional tables of thermodynamic and transport properties were interpolated using chamber pressure P_0 and mean *O/F* ratio as lookup variables. Calculated parameters included the gas constant R_g, ratio of specific heats γ, and flame temperature T_0. Defining the combustion efficiency as

$$\eta^* = \frac{c^*_{actual}}{c^*_{ideal}} = \frac{\sqrt{\left(\frac{\gamma+1}{2 \cdot \gamma} \right)^{\frac{\gamma+1}{(\gamma-1)}} R_g \cdot T_{0_{actual}}}}{\sqrt{\left(\frac{\gamma+1}{2 \cdot \gamma} \right)^{\frac{\gamma+1}{(\gamma-1)}} R_g \cdot T_{0_{ideal}}}} \approx \sqrt{\frac{T_{0_{actual}}}{T_{0_{ideal}}}} \quad , \tag{5}$$

the theoretical flame temperature $T0_{ideal}$ was scaled by adjusting the combustion efficiency

$$T_{0_{actual}} = \eta^{*2} \cdot T_{0_{ideal}} \quad , \tag{6}$$

such that the calculated fuel mass consumption

$$\Delta M_{fuel} = \int_0^t \left(\dot{m}_{total} - \dot{m}_{ox} \right) dt \tag{7}$$

matched the measured value from differences of the pre- and post-test weight measurements. As described earlier, the consumed fuel mass anchored the thermodynamic calculations.

Adjusting input combustion efficiency upwards has the effect of increasing the calculated fuel mass consumption, and downwards decreases the calculated fuel mass consumption. The calculations of Equations (3-7) were iterated, adjusting η^* after each iteration, until the calculated fuel mass matched the measured mass within a prescribed level of accuracy, in this case 0.5%. For each iteration, the time-averaged *oxidizer-to-fuel* ratio was calculated as integrated oxidizer massflow divided by the consumed fuel mass,

$$\overline{O/F} = \frac{\int_0^{t_{burn}} \dot{m}_{ox}(t) \cdot dt}{\Delta M_{fuel}} = \frac{\int_0^{t_{burn}} \dot{m}_{ox}(t) \cdot dt}{\int_0^{t_{burn}} \left[\dot{m}_{total}(t) - \dot{m}_{ox}(t) \right] \cdot dt} \tag{8}$$

Equivalence ratio was calculated by

$$\Phi = \frac{O/F_{stoichiometriuc}}{O/F_{test}} \quad , \tag{9}$$

The stoichiometric *O/F* ratio for each propellant combination was calculated using CEA.

The 1-dimensional de Laval flow equations (Anderson [32], Chapter 4) were used to calculate the thruster performance parameters. Thrust and thrust coefficient were calculated from chamber pressure as

$$F_{thrust} = P_0 A^* \cdot \left(\sqrt{\frac{2}{\gamma - 1} \cdot \left(\frac{2}{\gamma + 1} \right)^{\frac{\gamma+1}{\gamma-1}}} \left(1 - \frac{p_{exit}}{P_0} \right)^{\frac{\gamma-1}{\gamma}} + \left(\frac{A_{exit}}{A^*} \right) \left(\frac{p_{exit} - p_\infty}{P_0} \right) \right) , \tag{12}$$

$$C_F = \frac{F_{thrust}}{P_0 A^*} = \gamma \sqrt{\frac{2}{\gamma - 1} \cdot \left(\frac{2}{\gamma + 1} \right)^{\frac{\gamma+1}{\gamma-1}}} \left(1 - \frac{p_{exit}}{P_0} \right)^{\frac{\gamma-1}{\gamma}} + \left(\frac{A_{exit}}{A^*} \right) \left(\frac{p_{exit} - p_\infty}{P_0} \right) \tag{13}$$

Specific Impulse, Characteristic Velocity, and Impulse density were calculated as

$$I_{sp} = \frac{F_{thrust}}{g_0 \dot{m}_{total}} \quad , \tag{14}$$

$$c^* = \frac{P_0 \cdot A^*}{\dot{m}_{total}} \quad , \tag{15}$$

and

$$\rho I_{sp} = s_g \cdot g_0 \cdot I_{sp} \tag{16}$$

In Eq. (16) g_0 is normal acceleration of gravity at sea level, *9.8067 m/s²*. The thrust coefficient C_F and specific impulse I_{sp} were also calculated directly from the thrust sensed by the test stand load cell. Values calculated from both sources will be presented later in order to support the verisimilitude of the collected test data.

RESULTS AND DISCUSSION

This section presents results from the testing campaign. Results from tests using GOX and Nytrox will first be presented individually and then compared. For both test series, the oxidizer regulator set-pressure was adjusted such that the nozzle exit pressure was near the optimal (ambient) condition. The venturi flow meter was calibrated using cold flows for both GOX and Nytrox. Compressible flow equations (Anderson [32] Chapt. 4) were used to calculate the oxidizer massflow rates through the venturi.

Baseline O_2 Hot Fire Test Summary

As stated previously, a series of hot fire tests were performed using GOX as the oxidizer in order to establish a baseline for the small thruster system. Figure

12 plots the time histories from a typical GOX baseline test. Plotted are (a) Thrust, (c) Chamber Pressure, (c) Massflow, and (d) Consumed Propellant Mass.

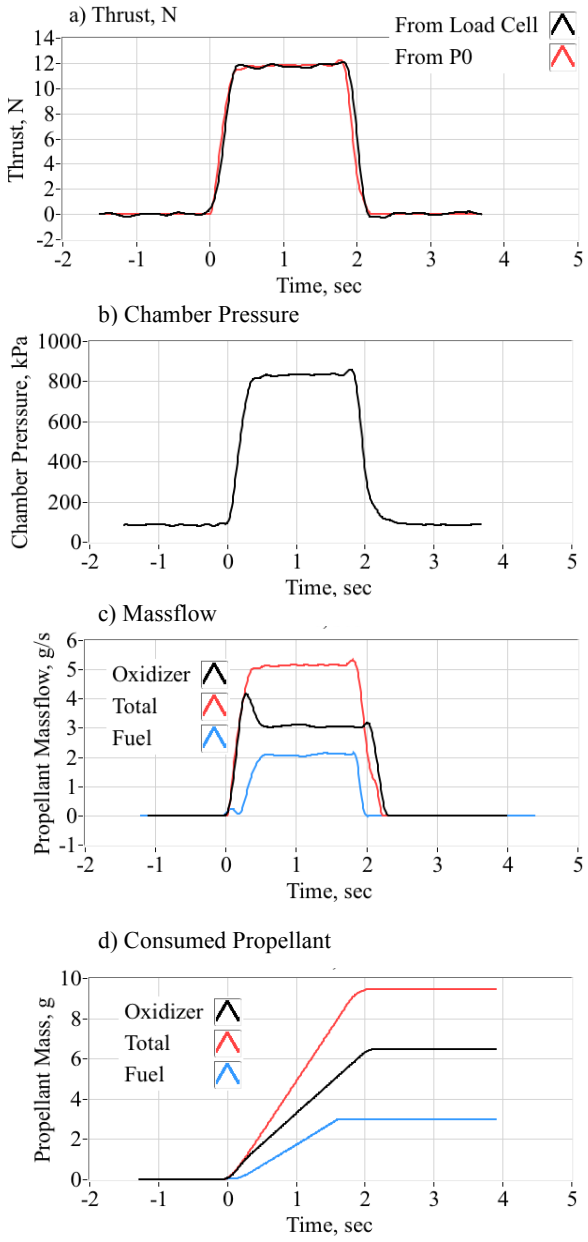

Figure 12. Baseline GOX/ABS Hot-Firing Time History.

The fuel massflow and consumed mass time histories were calculated using the procedure laid out in the previous section. Note that although the oxidizer flow initiates at time zero, the steady chamber pressure is not reached until approximately 300 msec later. The initial GOX time history overshoot is likely due to an unchoked nozzle as gas streams into the thrust chamber. On Fig. (12a) thrust values as directly measured by the load call and as calculated from chamber pressure using Eq. (12) show excellent agreement. This close comparison indicates that values for the nozzle-flow thermodynamic parameters, T_0, γ, M_w, *and* R_g, derived from the previously-described procedure are accurately calculated.

Figure 13 graphically summarizes the baseline tests, showing the results of 13 hot-firings. Results from 13 hot-firings are reported here. Plotted are I_{sp}, c^*, and C_F. The plotted test data are time-averages from the steady-state portions of each hot-fire test. For the purpose of this calculation the term "steady-state" means all data point that lie within 10% of the maximum observed thrust and chamber pressure levels.

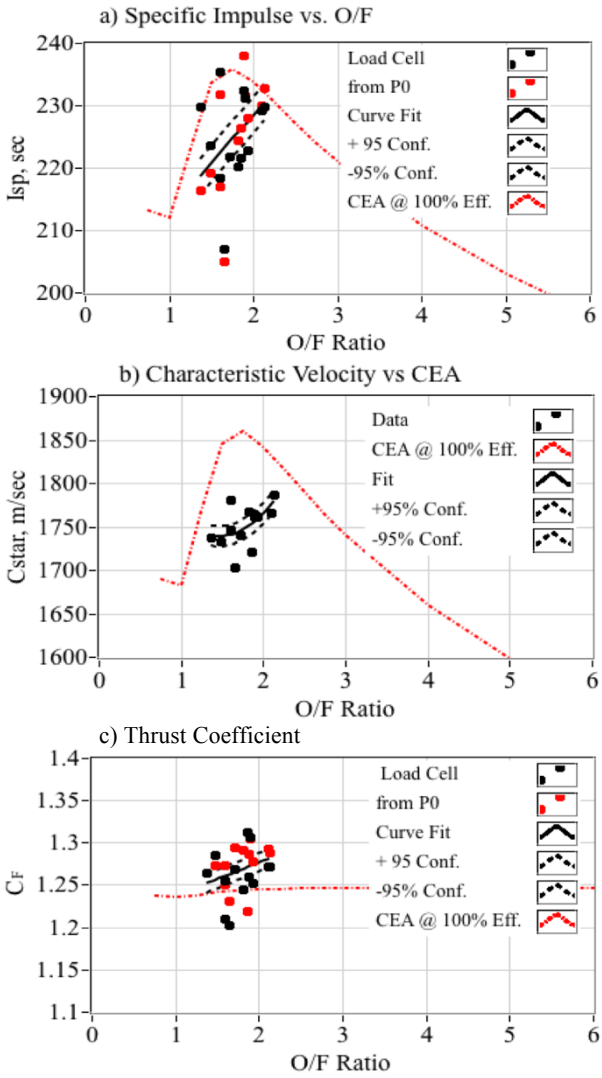

Figure 13. Summary of the GOX/ABS Baseline Test Results.

The specific impulse and thrust coefficient graphs also plot the values calculated using both the sensed thrust

from the load cell (black symbols), and the thrust calculated from chamber pressure (red symbols), as per Eqs. (12) and (13). Dashed red lines overlaid on the are I_{sp}, C_F, and c^* plots were values calculated from CEA assuming frozen flow at the nozzle throat. Based on the data of Fig. (13c) the GOX/ABS thruster achieved approximately 92% combustion efficiency.

Nytrox 87 Hot Fire Test Summary

Figure 14 plots the time histories from a typical hot-fire test. As with the previous plots of Fig. (12), the plotted time histories are (a) Thrust, (b) Chamber Pressure, (c) Massflow, and (d) Consumed propellant mass. The time scales of Fig. (14) have been skewed so that the zero-time point corresponds with the motor-ignition, signaled by a sharp rise of the chamber pressure. The nytrox run valve was opened approximately *400 ms* prior to full the motor ignition. This ignition latency was observed for the majority of the Nytrox tests, and reasons for this issue will be described in detail later in this section.

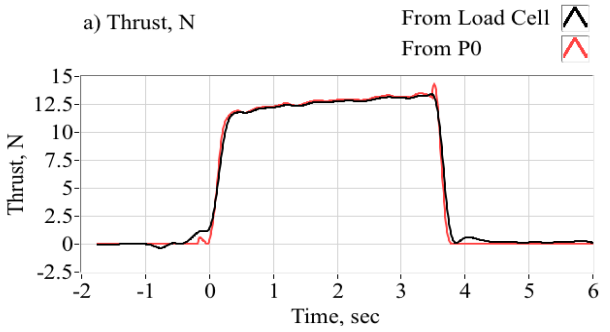

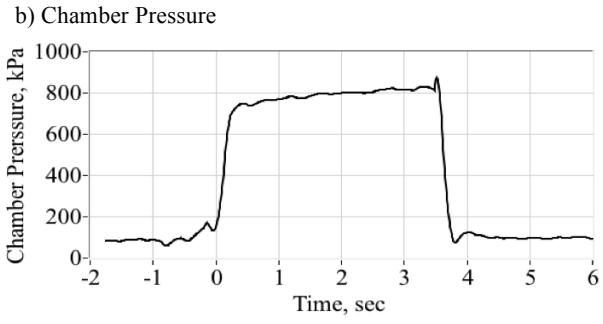

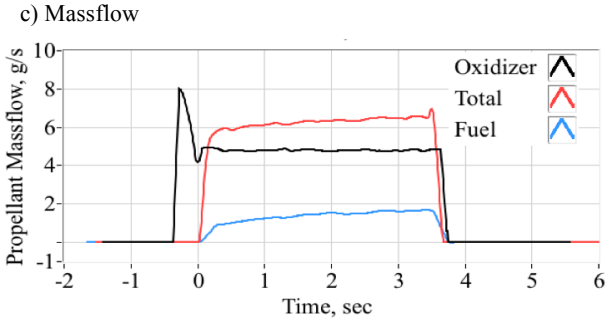

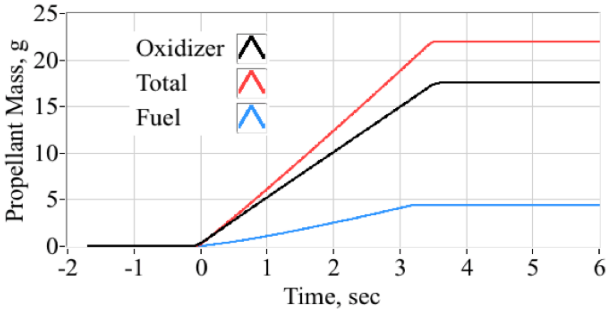

Figure 14. Nytrox /ABS Hot-Firing Time History.

Figure 15 graphically summarizes the Nytrox test results. Data from a total of 19 Nytrox hot-firings are reported. Fig. (15) plots I_{sp}, c^* *and* C_F, as a function of O/F ratio. Compared to the baseline GOX/ABS tests the values for I_{sp} and c^* drop by slightly more than 10%. Based on the theoretical calculations of Fig. (5), this drop was expected. Similar to the GOX/ABS burns, the data of Fig. (15c) shows that the Nytrox/ABS thruster achieved approximately 92% combustion efficiency.

Comparing Figs. (13a) for GOX and (15b) for nytrox, it is also apparent that the Nytrox motor tends to run slightly fuel-richer than optimal compared to GOX. Since the thruster had been previously optimized for best *O/F* ratio based on GOX, and the Nytrox oxidizer was simply "dropped in" as a replacement this result was not unexpected. The "drop in" inefficiency is also reflected by the thrust coefficient comparisons of Fig (13c) and (15c). Minor modifications to the thrust chamber dimensions, and nozzle expansion ratio would correct this inefficiency.

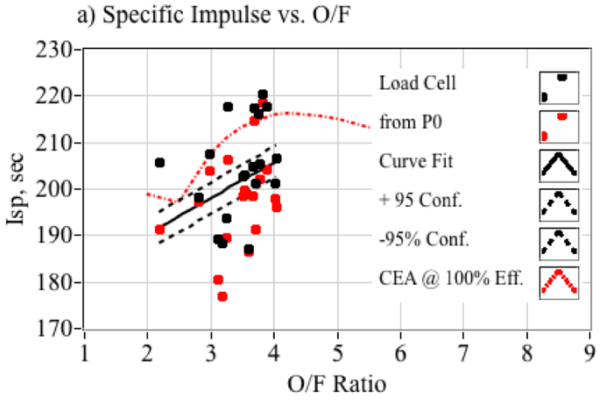

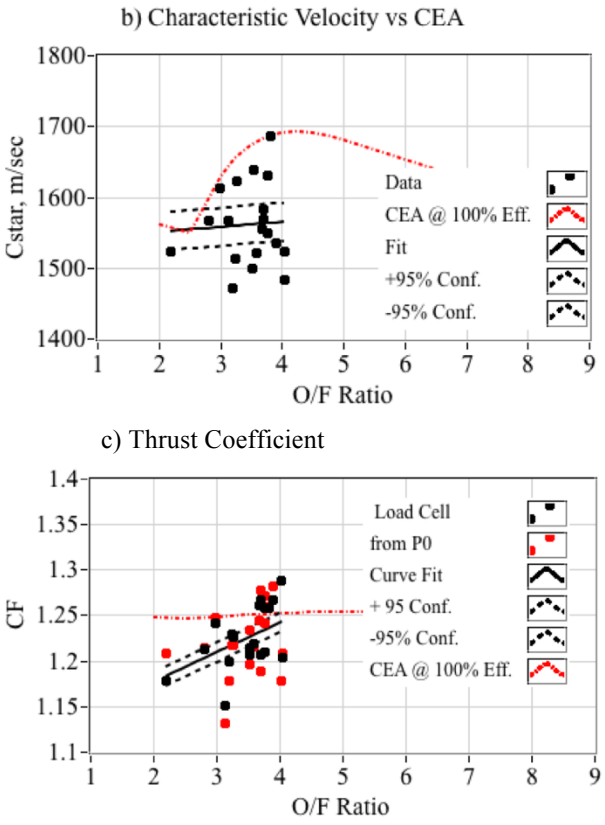

Figure 15. Summary of the Nytrox 87/ABS Hot Fire Test Results.

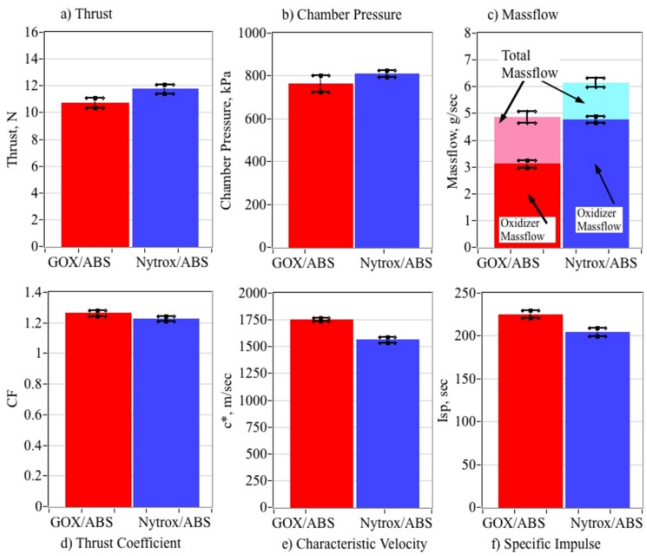

Figure 16. Comparing HPGHP Thruster System Performance using GOX/ABS and Nytrox 87/ABS Propellants.

GOX/Nytrox Burn Data Comparisons

This section compares the results of the GOX/ABS baseline against the Nytrox/ABS test results through a series of bar charts. Graphed are the mean values from each testing campaign as derived from the *13 GOX-baseline* and *19 Nytrox-evaluation hot fire tests*. Error bars, representing the 95-% student-t[33] confidence intervals for the appropriate degrees of freedom based on the number of measurements, are also plotted

Figure 17 bar charts compare the actual thrust, mean operating chamber pressure, oxidizer and total massflows, and performance parameters of the thruster using the two propellant classes. As shown by Figs. (*16a), (16b),* and (*16c)* the Nytrox oxidizer, inserted as a higher-density "drop in" for GOX results in slightly higher absolute thrust, chamber pressure, and massflow levels. These higher absolute levels result from the higher density of Nytrox 87 oxidizer, as compared to GOX.

In contrast the GOX/ABS thruster exhibits increased specific impulse I_{sp} and c^* level, compared to Nytro/ABS. For example, the mean GOX/ABS I_{sp} is approximately *224.8 sec* compared to *204.4 sec* Nytrox/ABS. The corresponding characteristic velocity values are *1751 m/s* and *1561 m/s, r*espectively. This lowered nytrox performance results from two factors, (1) the reduced optimal c^* for Nytrox/ABS based on a lower flame temperature, and (2) a less-than optimal *O/F* ratio for the nytrox/ABS thruster. The first factor was previously predicted by the analytical comparisons of Figure 5, and was expected. The second factor results from a less than efficient fuel grain geometry for the Nytrox/ABS combustion.

Figure 17 shows this efficiency comparison, plotting the ensemble mean O/F (a) and equivalence ratios (b). The corresponding stoichiometric O/F ratios are also plotted on Fug. (17a). The GOX/ABS thruster burned an equivalence ratio of approximately 1.65, which is spot-on the value for best performance. When Nytrox 87 *GOX* was swapped-in for GOX, the ensemble mean value for Φ is approximately 1.95, or slightly richer than would allow best performance. As described earlier, this inefficiency can be corrected by slightly shortening the fuel grain length in order to better approach the optimal O/F (or equivalence) ratio.

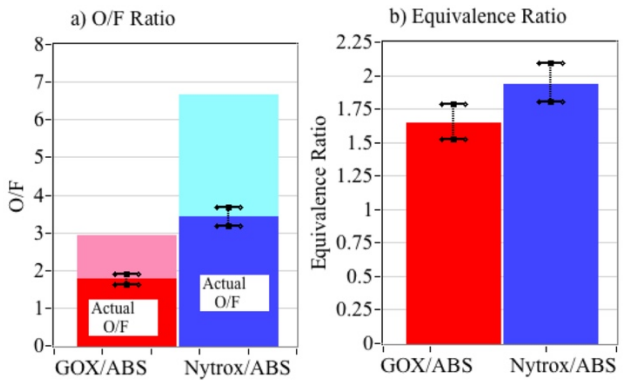

Figure 17. Comparing Combustion Properties of GOX/ABS and Nytrox 87/ABS Motors.

In contrast to the mass-based I_{sp} comparisons that favor the performance of the GOX/ABS propellants, the *Nytrox/ABS* propellants exhibit a significantly higher impulse density. The bar charts of Figure 18 show these comparisons. Plotted are effective specific gravity, Fig. (18a), and measured impulse density at ambient conditions, (18b). These values are based on the Nytrox liquid storage density at 86 atmospheres (from Peng-Robinson model) and 0^oC. The, the Nytrox/ABS propellants exhibit at least a 45% increase in volumetric efficiency when compared to GOX/ABS. As described previously, this result, predicted by the CEA analysis, was expected.

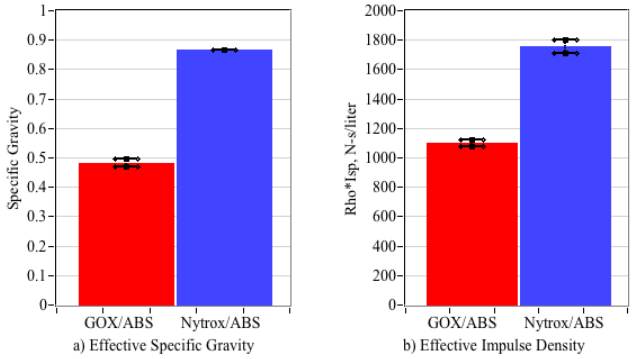

Figure 18. GOX/ABS and Nytrox 87/ABS Volumetric Efficiency Comparisons.

Extrapolating the Specific Impulse to Vacuum Conditions.

Recall that the specific impulse values plotted on Figs. (13), (15), and (16) were derived from data collected under ambient test conditions at approximately 4700 ft. (1,430 meters) altitude, the elevation of the test facility in Logan Utah. The 2.07:1 nozzle expansion-ratio was designed to give near-optimal performance at this altitude, and the desired operating chamber pressure.

Clearly, when matched with a high expansion-ratio nozzle, the vacuum performance will be significantly better. The ambient-test data can be extrapolated to altitude using the previously presented 1-D de Laval flow equations. (Anderson, Ref. [32]) For optimal operating conditions, the pressure thrust term of Eq. (13) vanishes and the ratio of the optimal and test I_{sp} can be written *as*

$$\frac{\left(I_{sp}\right)_{opt}}{\left(I_{sp}\right)_{test}} = \frac{\dfrac{P_0 \cdot A^*}{g_0 \cdot \dot{m}}\left(C_{F_{opt}}\right)}{\dfrac{P_0 \cdot A^*}{g_0 \cdot \dot{m}}\left(C_{F_{test}}\right)} = \tag{17}$$

$$\frac{\gamma \cdot \sqrt{\dfrac{2}{\gamma-1}\left(\dfrac{2}{\gamma+1}\right)^{\frac{\gamma+1}{\gamma-1}} \cdot \left(1-\left(\dfrac{\left(p_\infty\right)_{vac}}{P_0}\right)^{\frac{\gamma-1}{\gamma}}\right)}}{\gamma \cdot \sqrt{\dfrac{2}{\gamma-1}\left(\dfrac{2}{\gamma+1}\right)^{\frac{\gamma+1}{\gamma-1}} \cdot \left(1-\left(\dfrac{\left(p_{exit}\right)_{test}}{P_0}\right)^{\frac{\gamma-1}{\gamma}}\right)} + \left(\dfrac{A_{exit}}{A^*}\right)_{test} \cdot \left(\dfrac{\left(p_{exit}\right)_{test} - p_\infty}{P_0}\right)}} .$$

Using the mean thrust coefficient, chamber pressure, and combustion efficiencies, taken from Figs. (13) and (15), Figure 19 plots the specific impulse extrapolations for GOX/ABS and Nytrox 87/ABS. The plotted parameters are *(a)* optimal expansion ratio as a function altitude, *(b)* optimal C_F as a function of the optimal expansion ratio, *(c)* optimal I_{sp} as a function of expansion ratio, and *(d)* optimal impulse density as a function of altitude. Also plotted as the red and blue symbols are the actual experimental values for the *GOX/ABS* and *Nytrox 87*/ABS motors.

The *GOX/ABS* data extrapolates to an I_{sp} of greater than 345 seconds under vacuum conditions, while the Nytrox/ABS data extrapolates to just over 300 seconds. This I_{sp} value, although 8% lower than for *GOX/ABS,* is still nearly 25-30% higher than can be achieved by any of the "green" ionic liquid propellants or by hydrazine. Using a similar process to scale the impulse density, the corresponding optimal vacuum ρIs_p values are 1,590 N-s/liter for GOX/ABS, and 2,510 N-s/liter for Nytrox 87/ABS. These values will be compared to hydrazine and the ionic liquid "green" propellants AF-M315E[34] and LMP-103S[35] later in this report.

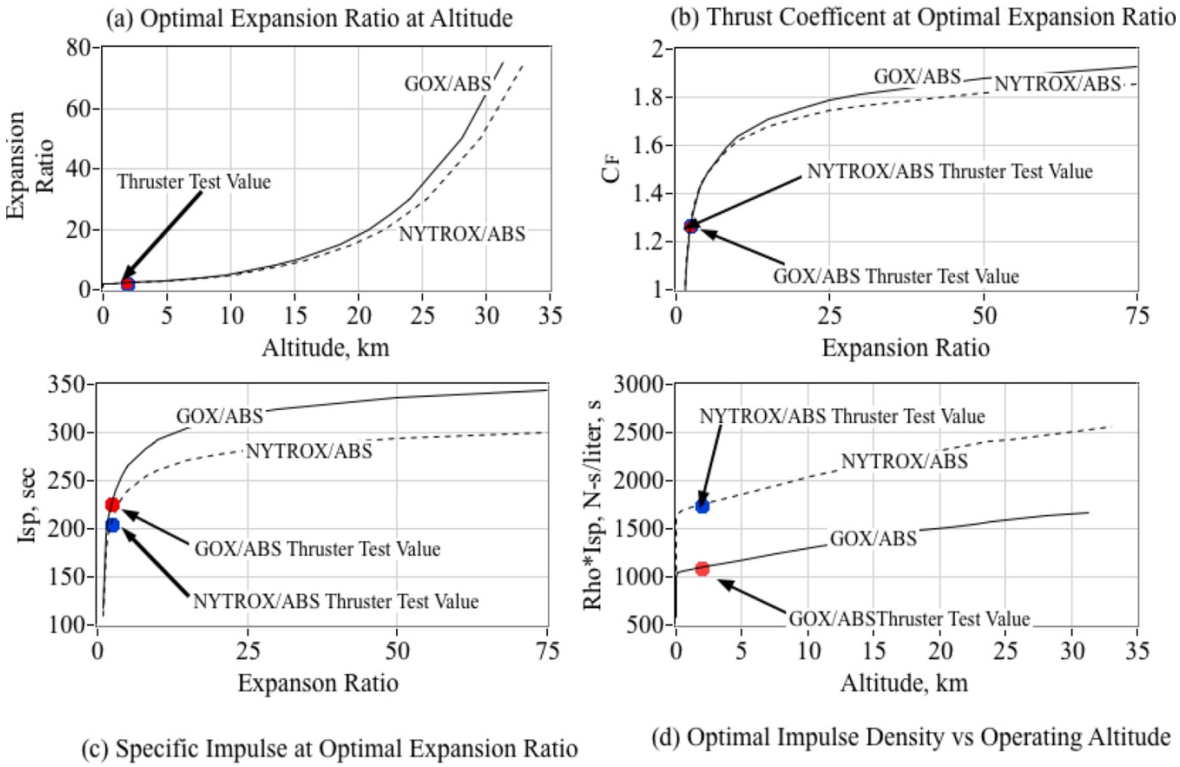

Figure 19. Extrapolating Ambient GOX/ABS and Nytrox 87/ABS Test Data to Optimal Vacuum Conditions.

Comparing the System Ignition Characteristics

As described in the introduction to this paper, one of the key objectives of this research campaign was to demonstrate that Nytrox, can be "dropped in" as a replacement for GOX, but still function effectively with the previously-matured arc-ignition system. In that regard, the arc-ignition system was effective in igniting the Nytrox/ABS propellants; but did exhibit several minor issues that must still be overcome for an operation system.

Ignition Energy

When a virgin fuel grain is first burned with Nytrox, the observed ignition reliability was only about 50%. "Setting" the arc path by first burning the grain using GOX, or by using a GOX pre-lead prior to initiating Nytrox flow overcame this problem. Once the first ignition is achieved, then the system reliably ignites using Nytrox, even with a dead-cold motor. The reason for this observed behavior appears to be that Nytrox expansion into the combustion chamber super-chills the ABS fuel, causing the surface impedance to increase to a point where the *HVPS* cannot provide sufficient power to pyrolize a conduction path through the virgin fuel material. Once a conduction path is set into the fuel material after the initial burn, then this issue goes away.

The data presented by Figure 20 supports this assertion. Here the required ignition energy is plotted as a function of the cumulative fuel grain burn lifetime. Recall from the previous discussion that the HVPS is current limited at 30 mA, and the output voltage is a function of the impedance path that the arc carves along the material surface. Total ignition energy is calculated as the integral of the output power. The HVPS output power is calculated as the product of the voltage and current-sense readings.

Fig. (20a) plots the ignition energy for GOX/ABS propellants, and Fig. (20b) plots the ignition energy for Nytrox/ABS as a function of cumulative burn time for the fuel grain. These data were taken from the burns plotted on Figs. 13 and 15. The first two points on Fig. (20b) near zero burn lifetime, were obtained from successful Nytrox tests of two previously unburned fuel grains without the GOX pre-lead. Both of these point show a considerably higher ignition energy requirement.

The remaining lower ignition energy data points plotted on Fig. (20b) were obtained from fuel grains that had been initially burned using a GOX pre-lead. For both GOX/ABS and Nytrox/ABS, the ignition energy correlates directly with burn time, indicating that the arc-path becomes better established, and the impedance drops following each ignition.

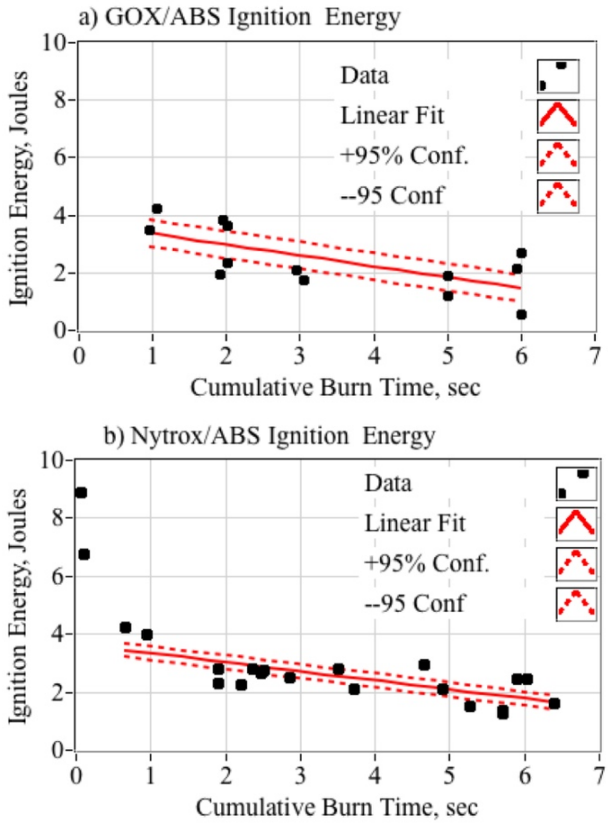

Figure 20. Effect of Fuel Grain Burn Lifetime on Required Ignition Energy.

Once the path is set, the required ignition energy is similar for both oxidizers. Excluding the virgin grain data, both systems have a mean startup energy less than 2.5 joules, and to a 95% confidence level, neither require more than 4 joules for ignition. This energy level is contrasted to the ECAPS Prisma[36] spacecraft which used the ADN-based LMP-103s green propellant. For first ignition this system required a 10 watt preheat for as long as 20 minutes, consuming more than 12,000 joules of energy.

Ignition Latency

As described earlier when the Nytrox solution is dropped into the HPGHP as the oxidizer, a considerable increase in ignition latency was experienced. The comparisons of Figure 21 illustrate this occurrence. Plotted are typical GOX/Nytrox/ABS burn time histories for of (a) thrust, (b) chamber pressure, (c) oxidizer massflow, and (d) Ignition Power. The Nytrox thruster ignition latency is readily apparent. The GOX/ABS motor lights and reaches within 63.2% of full operating pressure within about 150 milliseconds. In contrast the Nytrox/ABS Motor exhibits a more significant startup latency, in this example an additional 250 ms, or a total ignition latency of 400 ms.

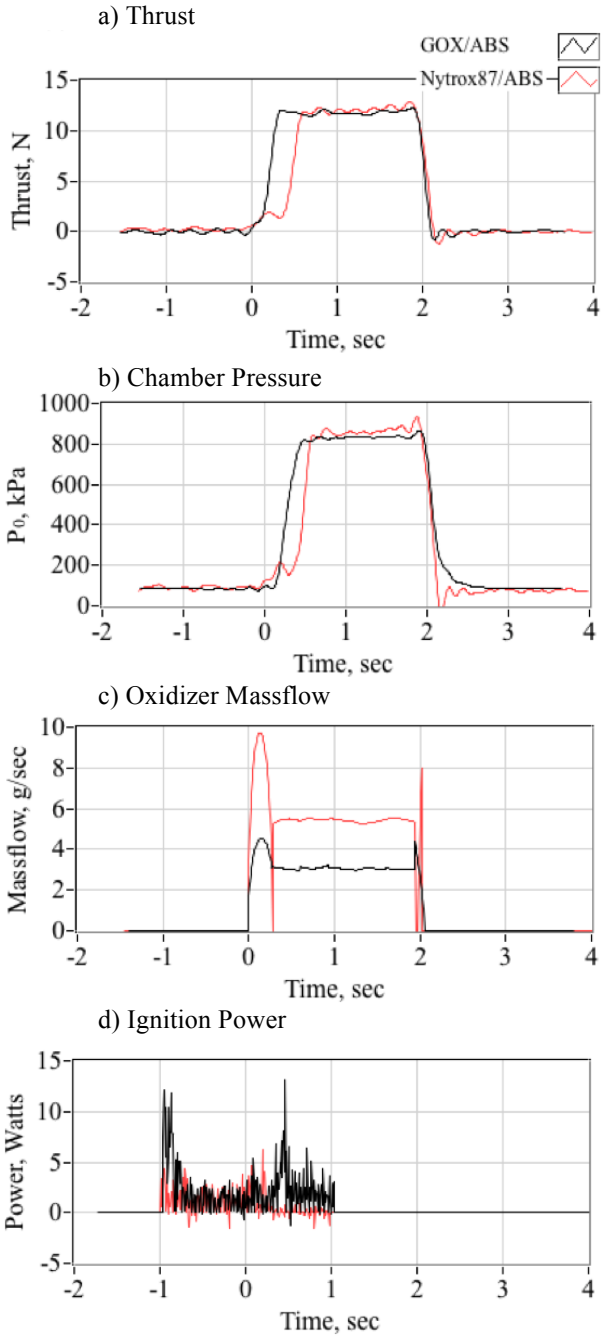

Figure 21. Comparing Typical Ignition Response Time Histories for GOX/ABS and Nytrox 87/ABS Thrusters.

In general, latency exhibited by the Nitrox/ABS propellants occurred for all of the test runs. The bar chart of Figure 22 compares the ensemble mean ignition latencies, calculated as the 63.2% first-order response rise time, using GOX and Nytrox as the oxidizer. Here

the mean ignition latency for the GOX-based system is approximately 300 msec, compared to approximately 825 msec for Nytrox.

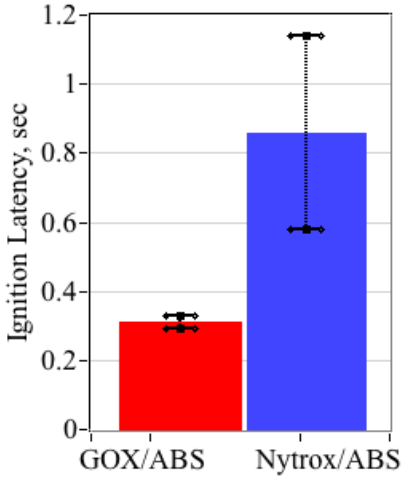

Figure 22. GOX/ABS, Nytrox/ABS Mean Ignition Latency Comparisons.

It is likely that this additional results from using the single-port GOX injector designed for the flow of a gaseous oxidizer. It appears that prior to ignition, super-chilled, mostly liquid, nytrox streams into the motor head-end, and it was necessary for this liquid to vaporize prior to full ignition. A redesign of the injector to provide multiple ports for better atomization and a swirl injection pattern for better mixing would likely eliminate or significantly reduce this latency. *This solution is recommended as a topic for further discovery.*

Comparing Nytrox to Existing Space Mono-Propellants.

With 19 successful hot-firings reported in this paper, *Nytrox* has been demonstrated as a reliable on- "drop-in" replacement for GOX in the *HPGHP* thruster system. Table 2 compares the performance of the Nytrox/ABS system to the competing propellants: hydrazine, and the emerging ionic-liquid "green" LMP-103S and AFM315-E.

Table 2. Nytrox/ABS Performance Characteristics Compared to Existing Space Mono-Propellants

Propellant	**Hydrazine** [37]	**LMP-103S** [37]	**AF-M315E**[37]	**Nytrox/ABS Hybrid**
Flame Temperature	600-750 ^oC	1600 ^oC	1900 ^oC	3000 ^oC
Vacuum $I_{sp,}$ *s*	220-225	252 (theory) 235 (delivered)	266 (theory) 245 (delivered)	320 (theory) 294 (extrapolated)
Specific Gravity	1.01	1.24	1.465	0.650 (87% N_2O)
Impulse density, *N-s/liter*	2270	3125 (theory) 2915 (delivered)	3900 (theory) 3650 (delivered)	2,510 (vacuum, extrapolated) 1750 (ambient, delivered)
Preheat Temperature	315 ^oC, cold-start capable	300 ^oC	370 ^oC	N/A none-required
Required Ignition Input Energy, *Joules*	N/A	12,000 J (10 Watts @ 1200 seconds)	27,000 J (15 Watts @ 1800 seconds	2.5 J (5 Watts for 500 ms)
Propellant Freezing Temperature	1-2 ^oC	-7 ^oC	< 0 ^oC *(forms glass, no freezing point)*	-70 ^oC
Cost	$	$$$	$$$$	$
Availability	Readily Available	Restricted Access	Limited Access	Widely Available
NFPA 704 Hazard Class				

The NFPA 704 Hazard[38] diamonds of Table 2 show the relative hazard levels of the various propellants. This NFPA hazard rating system includes three color codes and five intensity levels. Each color code (blue, red, and yellow) of the hazard rating system corresponds to a hazard: health, fire, and instability (denotation or chemical change). Within each colored section, a numerical rating is given to the hazard. The hazard ratings for AF-M315E are based on two noxious constituent components, Hydroxyl Ammonium Nitrate (*HAN*) and 2-Hydroxyethylhydrazine (*HEHN*).

With the exception of *impulse density*, the Nytrox/ABS system outperforms the other propellants in every listed category. Even the lower ρI_{sp} value is a bit misleading. Because Nytrox had the ability to safely self-pressurize, there is no need for an additional volumetrically inefficient oxidizer pressurization system. The absence of this secondary system significantly decreases the

overall system complexity, and leads to a clear advantage in volumetric efficiency. Due to the high pyrolysis energy of ABS fuel, 3.1 MJ/kg, the HPGHP motors are ablative and self-cooling, offering a final systems advantage.

SUMMARY AND CONCLUSION

Over the past decade a novel High-Performance "Green" Hybrid Propulsion (*HPGHP*) system has been developed as an environmentally sustainable replacement for hydrazine, and other highly-toxic spacecraft propellants. *HPGHP* is enabled by recent advances in 3-D printing and leverages unique electrical breakdown characteristics of printed plastics like ABS and polyamide. Additive manufacturing changes the electrical breakdown properties, and when printed materials are presented with a sufficiently high, low-current voltage, electrical-arcing along the layered surface pyrolizes material and seeds combustion when an oxidizing flow is introduced. The system has been engineering to a high level of reliability with the number of possible ignitions limited only by the amount of fuel. Typical startup sequences require less than 2 joules; and once started, the system can be sequentially fired with no additional energy inputs required.

In its most mature form *HPGHP* uses gaseous oxygen as the oxidizer. Although gaseous oxygen is highly mass efficient, it is volumetrically inefficient due to its low specific gravity unless stored at very high pressures. In order to increase the *HPGHP* system volumetric efficiency, a two-phase blend of nitrous oxide and *oxygen,* "Nytrox," has been engineered as a higher-density "drop-in" replacement. Nytrox is similar to "laughing-gas" used for anesthesia applications and is blended by percolating *oxygen* under pressure into N_2O until the solution reaches saturation.

With 19 successful hot-firings reported in this paper, results from the preliminary test-and-evaluation campaign have demonstrated Nytrox as an effective replacement for GOX in the HPGHP system, exhibiting a slightly reduced specific impulse, but with significantly higher volumetric efficiency. Vacuum specific impulse values exceeding 300 seconds (extrapolated) are reported. This I_{sp} is significantly greater than can be achieved by hydrazine or the current generation of "green" propellants based on ionic-liquids, LMP-103S and AF-M315E. Because Nytrox had the ability to safely self-pressurize, there is no need for an additional volumetrically inefficient oxidizer pressurization system. This characteristic significantly decreases the overall system complexity.

A primary issue associated with using Nytrox a replacement for GOX as a hybrid oxidizer is a significant increase in the cold-start ignition latency. It is likely that this additional results from using the single-port GOX injector designed for the flow of a gaseous oxidizer. It appears that prior to ignition, super-chilled, mostly liquid, nytrox streams into the motor head-end. Thus, it is necessary for this liquid to fully vaporize prior before full ignition occurs. A redesign of the injector to provide multiple ports for better atomization and a swirl injection pattern for better mixing would likely eliminate or significantly reduce this latency. This solution is recommended as a topic for further discovery.

Acknowledgments

The author is especially grateful for the assistance of NASA Marshall Space Flight Center (MSFC) ER-23, by graciously provided access to the testing facilities used to collect vacuum chamber data for this project. I deeply appreciate MSFC employees Kevin Pedersen and Carlos Diaz for their assistance with laboratory vacuum tests, and to Mr. George Story for his technical support and expert advice.

REFERENCES

1. Bombelli, V., "Economic Benefits for the Use of Non-toxic Monopropellants for Spacecraft Applications, AIAA-2003-4783, *39th AIAA/ASME/SAE/ASEE Joint Propulsion Conference and Exhibit*, Huntsville, AL, July 2003. https://arc.aiaa.org/doi/10.2514/6.2003-4783

2. Haeseler, D., Bombelli, V., Vuillermoz, P., Lo, R., Marée, T., & Caramelli, F., "Green Propellant Propulsion Concepts for Space Transportation and Technology Development Needs," *ESA SP-557, Proceedings of the 2nd International Conference on Green Propellants for Space Propulsio*n, Cagliari, Sardinia, Italy, 7-8 June 2004. https://www.researchgate.net/publication/234265416_Green_Propellant_Propulsion_Concepts_for_Space_Transportation_and_Technology_Development_Needs

3. Anon., "Hazard Analysis of Commercial Space Transportation; Vol. 1: Operations, Vol. 2: Hazards, vol. 3: Risk Analysis," *U.S. Dept. of Transportation*, PB93-199040, Accession No.

00620693, May 1988. https://www.faa.gov/about/office_org/headquarters_offices/ast/.../hazard.pdf

4. Anon., "Department of Defense Interface Standard, Eletromagnetic Environmental Effects requirements for Systems, *MIL-STD-464*, http://www.tscm.com/MIL-STD-464.pdf, [Retrieved 20 September 2018].

5. Whitmore, *S. A.,* Inkley, *N. R.,* Merkley, *D. P.,* and Judson*, M. I.,* "Development of a Power-Efficient, Restart-Capable Arc Ignitor for Hybrid Rockets", *Journal of Propulsion and Power*, Vol. 31, No. 6 (2015), pp. 1739-1749. https://dio.org/10.2514/1.B35595.

6. Whitmore, S. A., "Three-Dimensional Printing of "Green" Fuels for Low-Cost Small Spacecraft Propulsion Systems," *Journal of Spacecraft and Rockets*, Vol. 54, No. 6 (2017), https://doi.org/10.2514/1.A33782

7. Palermo, E., "Fused Deposition Modeling: Most Common 3D Printing Method," *LIVESCIENCE*, 19 September 2013. Available online: https://www.livescience.com/39810-fused-deposition-modeling.html, [Retrieved 2 December 2019].

8. Whitmore, S.A.; Mathias, S.D., "Harvey, R. High Voltage Breakdown and Arc-Tracking Mechanism of Thermoplastics with Applications to Hybrid Rocket Arc- Ignition," *53rd AIAA/SAE/ASEE Joint Propulsion Conference*, Atlanta, GA, USA, 10–12 July 2017; AIAA 2017-4601, https://doi.org/10.2514/6.2017-4601.

9. Whitmore, S. A., and Anthony M. Bulcher, A. M., "Vacuum Test of a Novel Green-Propellant Thruster for Small Spacecraft", AIAA 2017-5044. *53rd AIAA/SAE/ASEE Joint Propulsion Conference*, *AIAA Propulsion and Energy Forum*, 2017. https://doi.org/10.2514/6.2017-5044

10. Whitmore, S. A., Inkley N., and Merkley D. P., "Restartable Ignition Devices, Systems, and Methods Thereof," US Patent 10,527,004 B2, Jan 7., 2020.

11. Whitmore, S. A., "Three-Dimensional Printing of "Green" Fuels for Low-Cost Small Spacecraft Propulsion Systems," *Journal of Spacecraft and Rockets*, Vol. 54, No. 6 (2017), https://doi.org/10.2514/1.A33782.

12. Whitmore, S. A., and Bulcher, A. M., "A Green Hybrid Thruster Using Moderately Enriched Compressed Air as the Oxidizer", AIAA 2018-4841, *2018 Joint Propulsion Conference*, *AIAA Propulsion and Energy Forum*, https://doi.org/10.2514/6.2018-4841

13. Whitmore, *S. A.,* Inkley, *N. R.,* Merkley, *D. P.,* and Judson*, M. I.,* "Development of a Power-Efficient, Restart-Capable Arc Ignitor for Hybrid Rockets", *Journal of Propulsion and Power*, Vol. 31, No. 6 (2015), pp. 1739-1749. https://dio.org/10.2514/1.B35595

14. Anon., "Safety Standard for Oxygen and Oxygen Systems," NSS 1740.15, *NASA Office of Mission Assurance*, Washington DC, January 1996. https://ntrs.nasa.gov/search.jsp?R=19960021046

15. Anon., "Occupational Safety and Health Guideline for Nitrous Oxide," US Department of Labor, Occupational Health and safety Administration, http://www.osha.gov/SLTC/healthguidelines/nitrousoxide/recognition.html, [Retrieved 21 September 2018].

16. Rhodes, G., W., "Investigation of Decomposition Characteristics of Gaseous and Liquid Nitrous Oxide," *Air Force Weapons Laboratory*, Report AD-784 602, Kirtland AFB, New Mexico, July 1974. https://www.freelists.org/archives/arocket/01-2014/pdfEE82jaPU9W.pdf

17. Zakirov, V.; Sweeting, M.; Goeman, V.; Lawrence, T. Surrey Research on Nitrous Oxide Catalytic Decomposition for Space Applications. SSC00-XI-6, *Proceedings of the 14th Annual AIAA/USU Conference on Small Satellites*, August 2000; Available online: https://digitalcommons.usu.edu/cgi/viewcontent.cgi?article=2109&context=smallsat. [Retrieved 5 May 2019).

18. Karabeyoglu, A.; Dyer, J.; Stevens, J.; Cantwell, B. Modeling of N_2O Decomposition Events, AIAA 2008-4933, *44th AIAA/ASME/SAE/ASEE Joint Propulsion Conference and Exhibit*, Hartford, CT, USA, 1-3 July 2008, https://doi.org/10.2514/6.2008-4933.

19. Bracken, A.B.; Broughton, G.B.; Hill, W. Equilibria for Mixtures of Oxygen and Nitrous Oxide and Carbon Dioxide and Their Relevance to the Storage of N2O/O2 Cylinders for Use in Analgesia. *J. Phys. D* **1970**, *3*, 1747–1758, https://doi.org/10.1088/0022-3727/3/11/325.

20. Karabeyoglu, M.A. Nitrous Oxide and Oxygen Mixtures (Nytrox) as Oxidizers for Rocket Propulsion Applications. *J. Prop. and Power* 2014, *30*, 696–706, https://doi.org/10.2514/1.b34768.

21. Borisov, A.; Troshin, K.Y. Critical Conditions for Nitrous Oxide Ignition. *Russ. J. Phys. Chem.* 2009, https://doi.org/10.1134/S1990793109040150.

22. Linstrom, P., Mallard, W., "*NIST Chemistry WebBook*," NIST Standard Reference Database Number 69, *National Inst. of Standards and Technology*, Gaithersburg, Maryland, 2018, http://webbook.nist.gov/(Retrieved 28 April 2020).

23. Peng, D.-Y.; Robinson, D.B. A New Two Constant Equation of State. *Ind. Eng. Chem. Fundam.* 1976, *15*, 59–64, https://doi.org/10.1021/i160057a011.

24. Zudkevitch, D.; Joffe, J. Correlation and Prediction of Vapor- Liquid Equilibria with the Redlich-Kwong Equation of State, *AIChE J.* 1970, *16*, 112–119, https://doi.org/10.1002/aic.690160122.

25. Gordon, S., and McBride, B. J., "Computer Program for Calculation of Complex Chemical Equilibrium Compositions and Applications," NASA Technical Report RP-1311, 1994. https://ntrs.nasa.gov/archive/nasa/casi.ntrs.nasa.gov/19950013764.pdf.

26. Stoddard, R.L., "Experimental Investigation of N2O/O2 Mixtures as Volumetrically Efficient Oxidizers for Small Spacecraft Hybrid Propulsion Systems," Master's Thesis, *Utah State University Digital Commons*, December 2019, https://digitalcommons.usu.edu/, [Retrieved May 2020].

27. Whitmore, S.A., Stoddard, R.L., "N2O/O2 blends safe and volumetrically efficient oxidizers for small spacecraft hybrid propulsion," *Aeronaut. Aerosp. Open Access J.* 2019, 3. https://medcraveonline.com/AAOAJ/AAOAJ-03-00097.pdf. [Retrieved 5 May 2020].

28. Anon., "Pure Gasses," Airgas, an Air Liquide Company, http://airgassgcatalog.com/catalog/, pages 39, 40 [Retrieved 2 May 2020]

29. Anon., "Cesaroni Pro-X, A Better Way to Fly, Pro38® hardware," http://pro38.com/products/pro38/pro38.php, [Retrieved 5 January 2020].

30. Anon., "ULTRAVOLT C Series High Voltage CAP-Charging Supplies," Advanced Energy, Inc., *https://www.advancedenergy.com/globalassets/resources-root/data-sheets/ultravolt-c-series-data-sheet.pdf* [Retrieved 9 May 2020].

31. Holley, "Nitrous Oxide Systems," https://www.holley.com/brands/nos/, [Retrieved 6 May 2020.]

32. Anderson, J. D., *Modern Compressible Flow*, 3rd Edition, *The McGraw Hill Companies, Inc.*, 2003, New York, Chapter 4, pp. 127-187. ISBN-13: 978-0072424430. https://libcat.lib.usu.edu/search/i0070016542

33. Beckwith, T. G., Marangoni, R. D., and Lienhard V, J. H., *Mechanical Measurements*, 6th Ed., Prentice Hall, 2006, pp.43- 73. ISBN-13: 978-0201847659, ISBN-10: 0201847655

34. Hawkins, T. W., Brand, A. J., McKay, M. B., and Tinnirello, M., "Reduced Toxicity, High Performance Monopropellant at the U.S. Air Force Research Laboratory," *AFRL-RZ-ED-TP-2010-219, 4th International Association for the Advancement of Space Safety Conference*, Huntsville, AL, 19-21 May 2010. *www.dtic.mil/dtic/tr/fulltext/u2/a522113.pdf*

35. Persson, M., Anflo, K., and Dinardi, A., "A Family of Thrusters for ADN-Based Monopropellant LMP-103S," AIAA-2012-3815, *48th AIAA/ASME/SAE/ASEE Joint Propulsion Conference & Exhibit,* 30 July - 01 August 2012, Atlanta, Georgia, 2012. https://doi.org/10.2514/6.2012-3815

36. Pokrupa, N., Anglo, K., and Svensson, O., "Spacecraft System Level Design with Regards to Incorporation of a New Green Propulsion System," *AIAA-2011-6129, 46th AIAA/ASME/SAE/ASEE Joint Propulsion Conference and Exhibit*, San Diego, CA, July 31-Aug 3, 2011. https://doi.org/10.2514/6.2011-6129.

37. Brand, A., " Reduced Toxicity, High Performance Monopropellant," AFRL-RZ-ED-VG-2011-326, *Presentation at the Green Propellant Workshop, Sweden*, 12-15 Sep 2011, pg. 23., https://apps.dtic.mil/dtic/tr/fulltext/u2/a554667.pdf.

38. Anon., "*National Fire Protection Association Hazard Identification System*," ACS Chemistry for Life, https://www.google.com/search?client=firefox-b-1-d&q=NFPA+Hazard+Class, [Retrieved 10 May 2020].